CHINESE OPTICS LETTERS

Vol. 22, No. 5 | May 2024

Dual-comb soliton rains based on polarization multiplexing in a single-walled carbon nanotube mode-locked Er-doped fiber laser

Yue Zhao (赵 悦)[1,2], Ying Qin (秦 莹)[1,2], Kailin Jia (贾凯琳)[1,2], Li Chen (陈 丽)[1,2], Guangwei Chen (陈广伟)[1,2*], Guoqing Hu (胡国庆)[1,2], Tengfei Wu (武腾飞)[3**], Huiyu Li (李慧宇)[1,2], Jingwen He (贺敬文)[4], and Zhehai Zhou (周哲海)[1,2]

[1] Key Laboratory of Modern Optoelectronic Measurement Technology in Mechanical Industry, Beijing Information Science and Technology University, Beijing 100192, China

[2] Key Laboratory of the Ministry of Education for Optoelectronic Measurement Technology and Instruments, Beijing Information Science and Technology University, Beijing 100192, China

[3] Changcheng Institute of Metrology & Measurement, Beijing 100095, China

[4] National Physical Experiment Teaching Demonstration Center, Beijing Jiaotong University, Beijing 100044, China

*Corresponding author: chenguangwei@bistu.edu.cn

**Corresponding author: tengfei.wu@163.com

Received November 16, 2023 | Accepted January 11, 2024 | Posted Online May 14, 2024

We experimentally demonstrate tunable dual-comb soliton rains in a polarization multiplexing fiber laser based on a single-walled carbon nanotube. The repetition frequency difference of dual-comb pulses is about 39 Hz, with a maximum extinction ratio of 29 dB. With suitable polarization states, one of the dual-comb pulses switches into soliton rain sequence with chirped isolating soliton trains. The signal-to-noise ratio reaches 61 dB, which is 11 dB higher than that of the normal dual-comb pulses. The intervals between chirped isolating solitons are distributed progressively, and the number of isolating solitons can be flexibly tuned from 2 to 11 by adjusting polarization state or pump power. Our work will provide support for further understanding of interaction dynamics of solitons and give a new route to the application of precision measurement.

Keywords: mode-locked fiber laser; soliton rains; dual-comb pulses; gain relaxation dynamics; single-walled carbon nanotube.

DOI: 10.3788/COL202422.051402

1. Introduction

Passively mode-locked fiber lasers are considered to be a powerful tool for generating and studying complex soliton dynamics due to their special nonlinear effects, especially in exploring multi-soliton dynamics[1,2], such as synchronized multiwavelength solitons caused by intracavity group delay modulation[3] and gain-guided solitons under the action of the cavity pulse peak clamping effect[4]. At the same time, under the action of soliton shaping of dispersive waves, various multi-soliton forms such as high-order harmonic mode-locked soliton states and noise-like pulses appeared[5].

Dual-comb pulses with different repetition rates as one of the multipulse states are widely used in high-precision distance measurement[6], spectral monitoring[7], three-dimensional measurement, and coded imaging[8]. The dual-comb light source can be generated in both active and passive ways, such as active mode-locking generation using acousto-optic modulation or electro-optic modulation[9], or passive mode-locking generation using saturable absorbers (SAs) to generate two sets of optical frequency combs in the same resonator[10]. It can also be generated by two mode-locked lasers[11]. Based on the comprehensive consideration of structure, cost, and function, in recent years, single-cavity dual-comb mode-locked lasers have received extensive attention due to their simple structure, strong stability, low cost, and the ability to generate asynchronous pulses with high common-mode noise suppression and strong relative frequency stability[12]. Polarization multiplexing is one of the main methods of generating single-cavity dual-combs[13]. This refers to a pulse sequence with orthogonal polarization states, for which the nonlinear effects in each polarization state cannot compensate for the group velocity mismatch caused by the birefringence effect of the optical fiber, resulting in asynchronous pulses with different repetition

frequencies. The multi-output of a polarization multiplexed dual-comb fiber laser is two relatively stable asynchronous pulse sequences, but it still has rich dynamic characteristics. It can be applied to wireless transmission, coherent optical communication, and other fields[14,15].

The unique properties of the asynchronous pulse sequence in the polarization-multiplexed dual-comb pulse laser provide favorable conditions for the formation of multi-soliton pulses. When the continuous-wave noise background reaches a certain threshold, the soliton pulse will form and gather to the condensed phase to form a quasi-stable mode, called soliton rain[16]. Its formation is closely related to the coexistence of dissipative solitons and quasi-continuous background in a laser cavity. Since the soliton rain was observed in the anomalous dispersion erbium-doped fiber (EDF) laser, its generation and change process have gradually begun to be of concern[16,17]. The research on soliton rain focused on the fiber laser cavities under different gain mediums, locking modes, and dispersion working areas. For example, the soliton rain under normal dispersion was observed in a passively mode-locked Yb-doped fiber laser with dual-filter based on an SA[18]. Net normal dispersion soliton rain was observed in passively mode-locked Yb-doped fiber lasers based on graphene oxide[19]. Soliton rain and its second-harmonic and third-harmonic phenomena were observed in a wavelength tunable nanotube mode-locked Tm-doped fiber laser[20]. Trapezoidal envelope pulses and soliton rains were observed in a mode-locked EDF laser with a MoS_2 SA on microfiber[21]. By introducing a microfiber junction, the square-wave-like pulse-emitting soliton rain was observed in an ultra-long EDF laser[22]. In the passively mode-locked EDF laser based on a graphene SA, the generation and transformation of noise-like pulses and soliton rain were observed[23]. Through nonlinear multimode interference technology, the soliton rain with isolated solitons and soliton bunches in a passively mode-locked fiber laser was demonstrated experimentally and theoretically[24]. To the best of our knowledge, most of the characterizations of soliton rain are concentrated in the single-pulse state, and the research on the characterization of soliton rain in the dual-comb pulse state is still very rare.

In this work, the generation of soliton rains in the dual-comb pulse based on polarization multiplexing is observed and recorded in a single-walled carbon nanotube (SWNT) mode-locked fiber laser. The laser cavity exhibits a dual-comb pulse in the time domain while the small repetition frequency difference is shown in the frequency domain; it formed in a quasi-stable fashion with both condensed phase solitons, drift solitons, and background noise. This state can be achieved by adjusting the polarization controller (PC). By adding an external polarization beam splitter (PBS) and PC, it is confirmed that the generation of the dual-comb pulse is indeed achieved from polarization multiplexing, which results in the group velocity difference caused by the birefringence in the cavity. We believe that the discovery of dual-comb soliton rain provides a reference value for the further study of soliton rain, and may also extend the further understanding of multi-soliton dynamics.

2. Experiments

The experimental setup of an SWNT-based polarization multiplexing fiber laser is shown in Fig. 1(a). We used the SWNTs as saturable absorbers to achieve passive mode locking. The total cavity length is ~21 m, in which ~8.5 m EDF is used as the gain medium, and ~5 m single-mode fiber (SMF) is added into the cavity to adjust the intracavitary dispersion. The group velocity dispersion coefficients of EDF are $-17.6\ \mathrm{ps}\ (\mathrm{nm}\cdot\mathrm{km})^{-1}$, while for SMF, they are $17\ \mathrm{ps}\ (\mathrm{nm}\cdot\mathrm{km})^{-1}$, and the total dispersion β_2 in the cavity is $-0.085\ \mathrm{ps}^2$. The laser is pumped by one 980 nm laser diode via a hybrid combiner of WDM, OC, and PI-ISO. The 10% output is extracted from the laser for measurement. The PC_1 in the cavity is used to adjust the polarization state of the laser cavity. In addition, PC_2 and a PBS are connected outside the cavity to study the polarization properties of two orthogonal polarized beams. We measured the output spectra and radio frequency (RF) with a spectrum analyzer (Anritsu, MS9710C) and a frequency spectrograph (Keysight, N9020A), respectively. The output pulse sequence is measured with a 13-GHz, 40-GS/s oscilloscope (Keysight, DSA91304A). In addition, we used an autocorrelator (APE, PulseCheck 150) to obtain the pulse width.

We prepared the SWNT SA by the liquid phase exfoliation method, where SWNT dispersion and polymer solution (polyvinyl alcohol, PVA) are mixed together. The characterization of SA is performed by field emission scanning electron microscopy (FESEM) [Fig. 1(b)] and Raman analysis [Fig. 1(c)], by dropping SWNT solution on a silicon wafer. The results show that it has good activity and integrity.

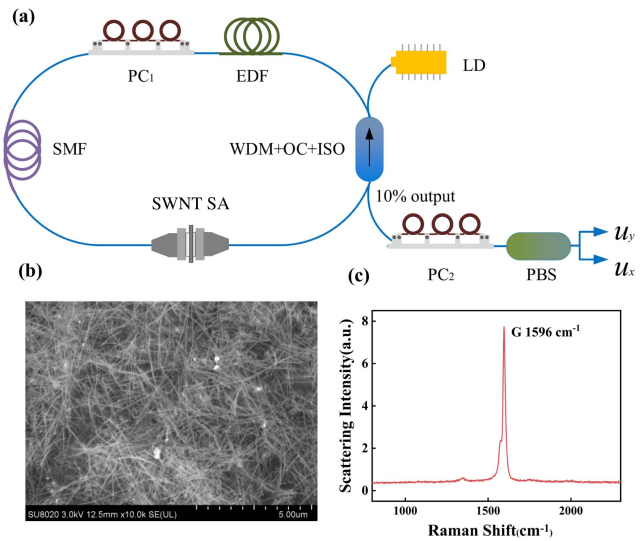

Fig. 1. (a) Schematic setup of an SWNT-based polarization multiplexing fiber laser. WDM, wavelength division multiplexer; OC, optical coupler; PI-ISO, polarization-insensitive isolator; PC, polarization controller; SWNT SA, single-walled carbon nanotube saturable absorber; EDF, erbium-doped fiber; SMF, single-mode fiber; PBS, polarization beam splitter; (b) FESEM analysis of SWNT; and (c) Raman analysis of SWNT taken at 532 nm excitation.

3. Results

When the pump current is adjusted to 80 mA, the laser achieves a stable mode-locked state. We then adjust the polarization state in the cavity and obtain a dual-comb pulse, as shown in Fig. 2. Figure 2(a) shows that the central wavelength of the output pulse is 1560 nm with 3 dB bandwidth of 4.03 nm. The fundamental frequency of the output pulses measured in the RF spectrum is near 9.89 MHz with a signal-to-noise ratio of about 50 dB, and the frequency difference is 39 Hz, as shown in Fig. 2(b). From Fig. 2(c), we can see that the two frequency components in the RF domain are shown as two asynchronous pulse sequences in the time domain, and the time period of two asynchronous pulses is about 100 ns.

If the low-intensity wave in the laser cavity is not completely filtered out, there will be a weak mode-locked state. In this state, the soliton pulse and the quasi-continuous background will coexist in the laser cavity, thus forming a unique multi-soliton state called soliton rains. The soliton rain pulse contains three field components, which are condensed phase, isolating solitons, and noise background. As for the meaning of the name, the formation process of soliton rain can be described as the following quasi-stable cycle mode. The interaction between multiple solitons will form a set of bound solitons, that is, condensed phase solitons. The combined effect of the radiation generated by the soliton and the CW mode in the cavity produces an inhomogeneous background. New solitons are generated from the background noise and converge on the condensed phase solitons. When the PC is adjusted to the appropriate position, the output characteristics of soliton rain are shown in Fig. 3. We can see obvious Kelly sidebands generated by the dispersive waves radiated by the solitons on both sides of the central wavelength, as shown in Fig. 3(a). The central wavelength of the output spectrum is 1560.6 nm with a 3 dB spectral bandwidth of 5.1 nm.

The time information displayed on the oscilloscope is shown in Fig. 3(b). It can be seen that there are two asynchronous pulse

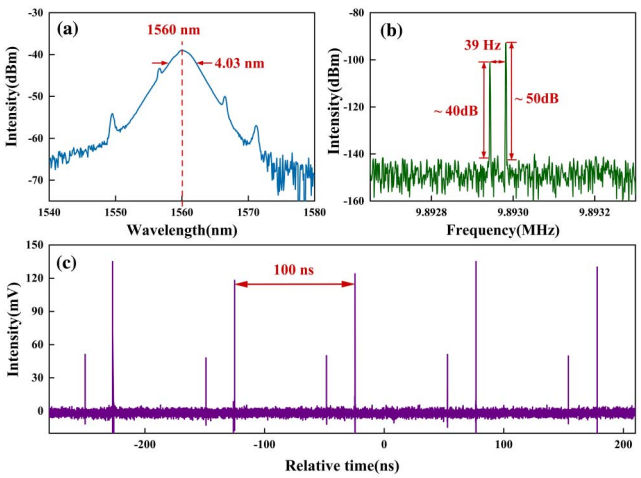

Fig. 2. Dual-comb state output information. (a) Output spectrum information; (b) RF spectrum with the resolution bandwidth of 1 Hz; (c) temporal information.

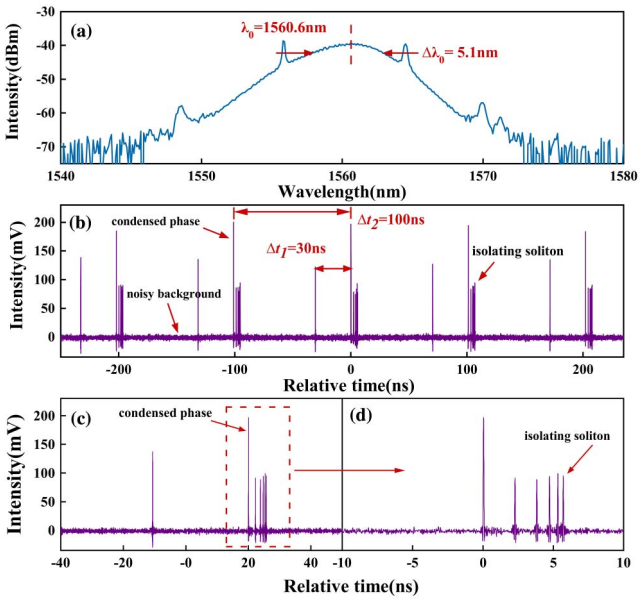

Fig. 3. Output characteristics of soliton rain. (a) Output spectrum information; (b) temporal information; (c), (d) detailed description of soliton rain pulse.

sequences in the captured temporal information, and the time interval between asynchronous pulses Δt_1 is 30 ns. On one of the pulse sequences, we can observe the soliton rain state and its three field components, which interact in the laser cavity and achieve dynamic balance. The time interval between the condensed phase solitons (pulse period) Δt_2 is 100 ns, corresponding to the length of the laser cavity. Figures 3(c) and 3(d) show the temporal information enlarged view of the soliton rain. It is not difficult to find from the enlarged diagram, in the direction away from the condensed phase, that the temporal interval between the isolating solitons gradually becomes smaller when they are further from the condensed phase, indicating that the isolating solitons are chirped soliton trains. This can be expressed by radiative waves and repulsive force between solitons. On the one hand, a small amplitude radiative wave of the sideband in the output spectrum can affect the separation between isolating solitons, where the separation is proportional to radiation[25–27]. On the other hand, the condensed phase drives the chirped soliton pulse forward, and the trailing pulses experience more gain than the leading pulses with the effect of gain relaxation dynamics. From Fig. 3(d), we can clearly see the quantitative characteristics of solitons. There are five isolated solitons in front of the condensed phase.

Because of the birefringence effect in the laser cavity, there is a group velocity difference between the mode-locked pulses in different polarization directions, which will cause the repetition frequency difference between the pulses. Corresponding to the asynchronous pulse on the oscilloscope, two similar frequency components can be observed on the frequency spectrum by properly adjusting the PC in the cavity. The RF spectrum and autocorrelation information in the soliton rain state are shown in Fig. 4. As shown in Fig. 4(a), the two frequency components are located at 9.892887 and 9.892942 MHz, respectively, with the

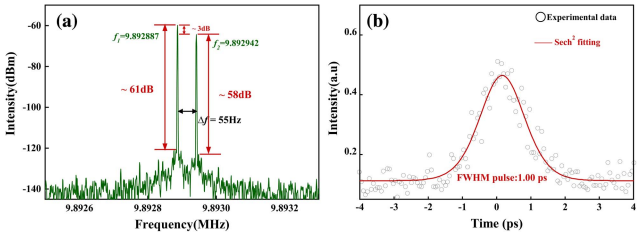

Fig. 4. RF and autocorrelation information in dual-comb mode-locking state. (a) RF spectrum of the dual-comb ultrashort pulses; (b) autocorrelation trace of output pulse and sech^2 fitting.

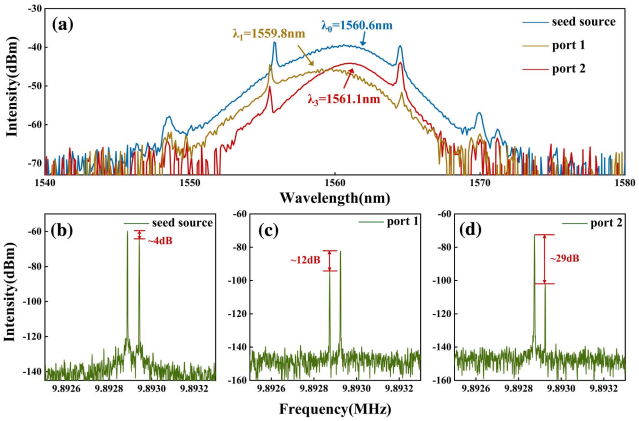

Fig. 5. (a) Spectral information of seed source and polarized light, and (b)–(d) RF spectra of seed source and polarized light.

resolution bandwidth of 1 Hz, which corresponds to the cavity length. The repetition frequency difference is 55 Hz. The signal-to-noise ratios of the two frequencies are ∼61 and ∼58 dB, respectively. Compared with that of Fig. 2(b), the signal-to-noise ratio of the dual-comb pulse in the soliton rain state is significantly enhanced, at ∼21 and ∼8 dB, respectively. The improvement of signal-to-noise ratio indicates that the laser operates close to the range of soliton rain, where the noise background is partially compressed. The output power of the laser cavity is 466 μW. Because of the insufficient saturation of EDF and intracavity loss (such as loss from hybrid device, SA, and fusion spliced loss), the output laser power is low and limits their practical application. But the dual-pump structure and fiber amplifier can enhance output power to cover the demand for precision measurement. In order to facilitate the measurement of pulse width, we connected a homemade EDF amplifier at the output end of the laser cavity. Figure 4(b) shows the autocorrelation trace of the output pulse, which is fitted by the sech^2 function. It can be seen that the full width at half-maximum (FWHM) of the pulse profile is 1.00 ps.

We speculate that the different states caused by the different establishment times of asynchronous pulses may be the main reason for the formation of dual-comb soliton rain. Because the polarization-dependent gain in the gain fiber will lead to the difference in the establishment time of each soliton[28], we know that the soliton rain pulse is formed in the metastable state, when one of the two asynchronous pulses achieves stable mode locking and the other is in the metastable state. Under the action of background noise, drift solitons will be generated near the metastable solitons according to their energy distribution, thus forming the soliton rain pattern, which may lead to the formation of a unique dual-comb soliton rain pulse.

In order to study the type and generation mechanism of two frequency components, we connect a PBS at the output end of the laser cavity. A PC also needs to be added in front of the PBS to eliminate energy coupling of polarized light. Because of the different transmittances of the polarization splitter to different polarization directions in the same beam, the light emitted by the laser will be separated into two linearly polarized beams with a polarization direction of 90° after passing through the PBS. This corresponds to an asynchronous pulse with slightly different relative velocities in the time domain. The information observed on the spectrometer and frequency spectrum after the PBS are shown in Fig. 5. Figure 5(a) records the spectral shapes of the direct output and the two polarized beams. The central wavelengths are shifted after polarization splitting, but they have similar shapes. The center wavelengths of port 1 and port 2 are 1559.8 and 1561.1 nm, respectively, with a difference of ∼1.3 nm. Both have soliton sidebands near 1555 and 1565 nm. We can observe that after polarization splitting, the 3 dB spectral bandwidth is less than 5.1 nm compared with the direct output. While adjusting the PC at suitable state, we can see a significant change in the height difference between the two frequency components in the RF spectrum. Figures 5(b)–5(d) show the relative changes of two frequency components of port 1 and port 2. The height differences of the two frequency components in the seed source, port 1, and port 2 are 4, 12, and 29 dB. The corresponding extinction ratios of port 1 and port 2 are 16 and 25 dB. This also proves that the two frequency components are indeed generated by polarization multiplexing effect.

Figure 6 records the asynchronous pulse sequence and pulse width information of the two polarized components. The temporal trains of the asynchronous pulse sequence are shown in Figs. 6(a)–6(c). The time intervals between the condensed phase solitons are 100 ns, and the time interval of the two asynchronous pulses is 30 ns. It can be seen that the relative intensity of the isolated solitons and the two asynchronous pulses has obviously changed. After the PBS, the intensity ratios of two asynchronous pulse sequences of the seed source, port 1, and port 2 are 2.37, 2.89, and 5.04, respectively. At the same time, the energy of the isolating soliton has also changed under different polarization states, but the numbers of isolating solitons at port 1 and port 2 are both five, which is the same as that of the seed source. Figures 6(d)–6(f) record the autocorrelation trace of the seed source and two polarized beams and their sech^2 fitting results. From the autocorrelation trace, we can see that the pulse widths of the two polarized beams are 1.34 and 1.01 ps, respectively. Compared with the direct output pulse, the width becomes slightly widened due to the dispersion broadening effect of external single optical fibers.

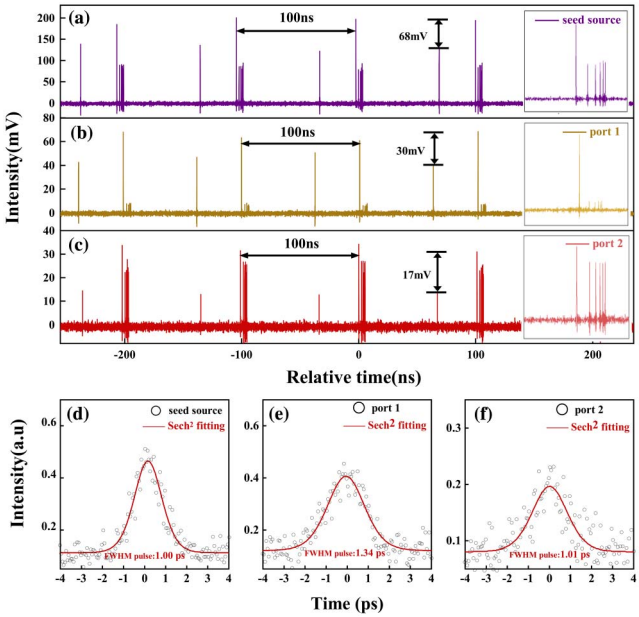

Fig. 6. Time domain and autocorrelation information of seed source and two polarization directions. (a), (b), (c) Asynchronous pulse sequence; (d), (e), (f) autocorrelation trace and sech^2 fitting.

To select a soliton count inside a molecule, Kokhanovskiy *et al.* introduced a 5-nm spectral filter and two independently pumped active mediums to an all-polarization-maintaining figure-of-eight fiber laser. The number of coherent solitons is adjustable between two and six. This method could effectively eliminate the polarization effects on environmental perturbations and has only two freedoms, which conveniently achieves tuning[29]. Similar to this adjustability, we experimentally verified the influence of different pump powers and polarization angles on the number of isolating solitons. When the pump current is increased to 85 mA, the number of isolating solitons

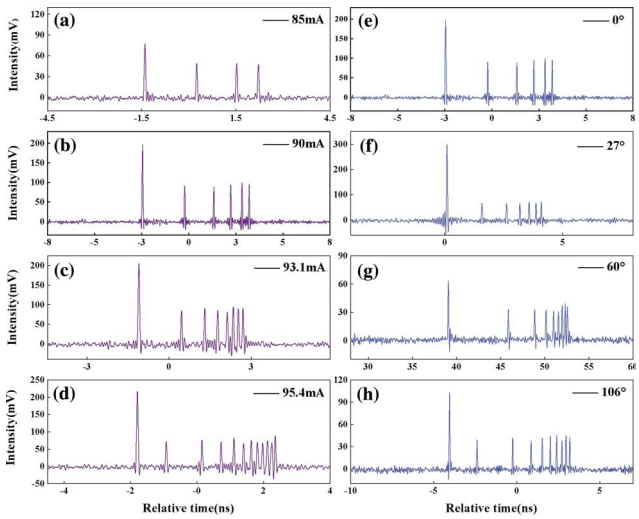

Fig. 7. Change in the number of isolating solitons under different pump currents and different PC angles. (a)–(d) Different pump currents; (e)–(h) different PC angles.

Table 1. Polarization Angle Corresponding to the Number of Different Isolating Solitons.

Number of Isolating Solitons	Rotating Angle of Paddle 1	Rotating Angle of Paddle 2	Rotating Angle of Paddle 3
5	0°	0°	0°
6	0°	0°	27°
8	0°	0°	60°
9	0°	0°	106°

separated from the condensed phase solitons is three, as shown in Fig. 7(a). When the pump current is further increased to 95.4 mA, we captured 5, 7, and 11 isolating solitons, as shown in Figs. 7(b)–7(d). This shows that the change of pump current is positively correlated with the change of isolating soliton. At the same time, when we adjust the states of PC_1, the number of isolating solitons is also varied.

The three-paddle PC utilizes the principle of tension-induced birefringence to produce three separate wave plates (fiber-optic delays); the phase delay of each paddle can be described as

$$\phi\,[\text{radians}] = \frac{2\pi^2 aNd^2}{\lambda D}.$$

Here, the phase delay is related to the number of winding turns N, fiber cladding diameter d, winding diameter D, and wavelength. In our experiment, the loop configuration of the PC includes 2-4-2 turns, the diameter of the fiber cladding is 125 μm, and the diameter of the circle is 35 mm. In order to display the polarization angle and phase more intuitively, we listed one of the ways to change the PC when the number of isolating solitons changed from five to nine, as shown in Table 1. When paddle 2 is constant and the angles between paddle 1 and paddle 3 are 0°, 27°, 60°, and 106°, the number of isolating solitons changed to five, six, eight, and nine, respectively. Here, we set it as 0° when the three paddles are closest to the experimental platform. The fiber winding tensions of paddles are measured as 15g, 14g, and 14g using a tensiometer.

When the pump current is 90 mA, the total angle of the PC is 0°, and we record five isolating solitons. When the angle is adjusted to 27°, there are six isolating solitons. Meanwhile, the number of isolating solitons of eight and nine corresponds to the polarization angle of 60° and 106°, obtained by rotating it clockwise. Figures 7(e)–7(h) display the number of isolating solitons at the mentioned four different polarization angles, which is five, six, eight, and nine, respectively. The experimental results demonstrate that the numbers of isolating solitons are flexible. In order to monitor the stable state of soliton rain, we record the maintenance of soliton rain under the polarization states plotted in Fig. 7. They could be maintained for at least 30 min before the PC needs to be reset again. As shown in Fig. 8, it can be seen that the soliton rain remains relatively stable in half an hour, with the number of isolating solitons being four and

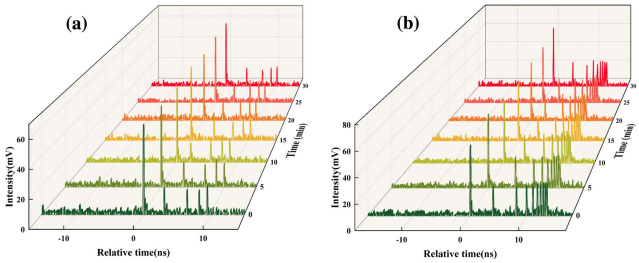

Fig. 8. Evolutions of soliton rain state (a) with four isolating solitons, and (b) with nine isolating solitons within 30 min.

nine. The convenient selection of the isolating soliton count in soliton rain will extend the application of dual-comb fiber lasers, in fields such as optical fiber sensing, ranging, radar detection, and coded imaging. But we should give sufficient attention to the drift of polarization states of PCs in practical application, particularly precise measurement. Intelligent control of mode-locked fiber lasers with machine learning and electrical PCs may be an effective way to address these issues.

4. Discussion

In summary, we observed the soliton rain phenomenon in the dual-comb pulse, which is based on the polarization multiplexing mechanism in the carbon nanotube mode-locked EDF laser. Under the different pump powers, we obtained the dual-comb pulse and the dual-comb soliton rain pulse. The repetition frequency difference is 39 and 55 Hz, respectively. Compared with the signal-to-noise ratio of the normal dual-comb pulse 50 dB, the dual-comb soliton rain pulse shows more stable characteristics, and the signal-to-noise ratio reaches 61 dB. At the same time, by adjusting the polarization angle and the pump current, we realized the number change of isolating solitons from two to eleven, and confirmed its tunability. Our experiments have confirmed that the formation of asynchronous pulses is under the mechanism of the polarization multiplexing. For the complex multi-soliton dynamics, especially the dynamics of soliton rain, the discovery of dual-comb soliton rain will possibly require more extensive study.

Acknowledgements

This work was supported by the National Natural Science Foundation of China (Nos. 62105036, 62105038, and 62005020) and the R&D Program of Beijing Municipal Education Commission (No. KM202211232020).

References

1. H. Zhang, D. Mao, Y. Du, *et al.*, "Heteronuclear multicolor soliton compounds induced by convex-concave phase in fiber lasers," Commun. Phys. **6**, 191 (2023).
2. N. N. Akhmediev, A. Ankiewicz, and J. M. Soto-Crespo, "Multisoliton solutions of the complex Ginzburg-Landau equation," Phys. Rev. Lett. **79**, 4047 (1997).
3. D. Mao, H. Wang, H. Zhang, *et al.*, "Synchronized multi-wavelength soliton fiber laser via intracavity group delay modulation," Nat. Commun. **12**, 6712 (2021).
4. L. Zhao, D. Tang, T. Cheng, *et al.*, "Generation of multiple gain-guided solitons in a fiber laser," Opt. Lett. **32**, 1581 (2007).
5. S. Huang, Y. Wang, P. Yan, *et al.*, "Soliton rains in a graphene-oxide passively mode-locked ytterbium-doped fiber laser with all-normal dispersion," Laser Phys. Lett. **11**, 025102 (2014).
6. Z. Zhu and G. Wu, "Dual-comb ranging," Engineering **4**, 772 (2018).
7. P. Fjodorow, P. Allmendinger, R. Horvath, *et al.*, "Monitoring formaldehyde in a shock tube with a fast dual-comb spectrometer operating in the spectral range of 1740–1790 cm^{-1}," Appl. Phys. B **126**, 193 (2020).
8. C. Wang, Z. Deng, C. Gu, *et al.*, "Line-scan spectrum-encoded imaging by dual-comb interferometry," Opt. Lett. **43**, 1606 (2018).
9. M.-G. Suh, Q.-F. Yang, K. Y. Yang, *et al.*, "Microresonator soliton dual-comb spectroscopy," Science **354**, 600 (2016).
10. D. Tang, H. Zhang, L. Zhao, *et al.*, "Observation of high-order polarization-locked vector solitons in a fiber laser," Phys. Rev. Lett. **101**, 153904 (2008).
11. V. Torres-Company and A. M. Weiner, "Optical frequency comb technology for ultra-broadband radio-frequency photonics," Laser Photonics Rev. **8**, 368 (2014).
12. X. Gu, G. Wang, Y. Li, *et al.*, "Polarization-multiplexed, single-cavity dual-comb fiber laser based on a birefringent crystal and a saturable absorber," Opt. Express **31**, 56 (2023).
13. Z. Zhu, Y. Liu, J. Yang, *et al.*, "A review of single-cavity dual-comb laser and its application in spectroscopy," Spectrosc. Spect. Anal. **41**, 3321 (2021).
14. K. Mallick, R. Mukherjee, B. Das, *et al.*, "Bidirectional hybrid OFDM based wireless-over-fiber transport system using reflective semiconductor amplifier and polarization multiplexing technique," Int. J. Electron. Commun. **96**, 260 (2018).
15. D. Pérez-Galacho, R. Zhang, A. Ortega-Moñux, *et al.*, "Integrated polarization beam splitter for 100/400 GE polarization multiplexed coherent optical communications," J. Light. Technol. **32**, 361 (2014).
16. S. Chouli and P. Grelu, "Rains of solitons in a fiber laser," Opt. Express **17**, 11776 (2009).
17. S. Chouli and P. Grelu, "Soliton rains in a fiber laser: an experimental study," Phys. Rev. A **81**, 063829 (2010).
18. C. Bao, X. Xiao, and C. Yang, "Soliton rains in a normal dispersion fiber laser with dual-filter," Opt. Lett. **38**, 1875 (2013).
19. S. Huang, Y. Wang, P. Yan, *et al.*, "Soliton rains in a graphene-oxide passively mode-locked ytterbium-doped fiber laser with all-normal dispersion," Laser Phys. Lett. **11**, 025102 (2014).
20. B. Fu, D. Popa, Z. Zhao, *et al.*, "Wavelength tunable soliton rains in a nanotube-mode locked Tm-doped fiber laser," Appl. Phys. Lett. **113**, 193102 (2018).
21. Z. Wang, R. He, Y. Liu, *et al.*, "Generation of trapezoidal envelope pulses and soliton rains from passively mode-locked fiber laser with MoS_2 saturable absorber on microfiber," Appl. Phys. Express **11**, 072504 (2018).
22. J. Zhou, J. Zhao, L. Li, *et al.*, "Microfiber knot assisted soliton rains emission from square-wave-like pulse in an erbium-doped fiber laser," in *14th Pacific Rim Conference on Lasers and Electro-Optics* (2020), paper P5_26.
23. P. Tang, M. Luo, T. Zhao, *et al.*, "Generation of noise-like pulses and soliton rains in a graphene mode-locked erbium-doped fiber ring laser," Front. Inform. Technol. Electron. Eng. **22**, 303 (2021).
24. G. Chen, K. Jia, S. Ji, *et al.*, "Soliton rains with isolated solitons induced by acoustic waves in a nonlinear multimodal interference-based fiber laser," Laser Phys. **33**, 035101 (2023).
25. J. M. Soto-Crespo, N. Akhmediev, P. Grelu, *et al.*, "Quantized separations of phase-locked soliton pairs in fiber lasers," Opt. Lett. **28**, 1757 (2003).
26. A. Hause, H. Hartwig, M. Bohm, *et al.*, "Binding mechanism of temporal soliton molecules," Phys. Rev. A **78**, 063817 (2008).
27. G. P. Agrawal, *Nonlinear Fiber Optics*, 4th ed. (Academic Press, 2007).
28. K. Zhao, C. Gao, X. Xiao, *et al.*, "Buildup dynamics of asynchronous vector solitons in a polarization-multiplexed dual-comb fiber laser," Opt. Lett. **45**, 4040 (2020).
29. A. Kokhanovskiy, E. Kuprikov, A. Ivanenko, *et al.*, "All-polarisation-maintaining modified figure-of-8 fibre laser as a source of soliton molecules," Laser Phys. Lett. **17**, 085101 (2020).